ChemPhysChem

Research Article
doi.org/10.1002/cphc.202400216

Chemistry Europe
European Chemical Societies Publishing

www.chemphyschem.org

From Lithium and Sodium Superoxides to Singlet-Oxygen – Insights into the Mechanism of Dissociation Using SHARC-MD

Dennis S. Pietruschka,[a, b] Aleksandr Zaichenko,[a, b] Martin Richter,[c] Stefanie Gräfe,[d] and Doreen Mollenhauer*[a, b]

The formation of highly reactive singlet oxygen from alkaline superoxides presents an important reactivity of this component class. Investigations of the reaction paths such as disproportionation of LiO_2 and NaO_2 have been presented. Furthermore, the dissociation of these superoxide systems have been discussed as an alternative reaction channel that also allows the formation of singlet oxygen. Here, we present a fundamental study of the electronic nature and dissociation behaviour of the alkali superoxides. The molecular systems were calculated at the CASSCF/CASPT2-level of theory. We determined the minimum energy crossing points along the dissociation required to form triplet oxygen $^3O_2$ and singlet oxygen $^1O_2$. Building on these results, a surface-hopping AIMD-simulation was performed employing the SHARC program package to follow the electronic transitions along the minimum energy crossing points during the dissociation. The feasibility of populating the electronic state corresponding to the formation of singlet oxygen during dissociation was demonstrated. For LiO_2, 6.85% of the trajectories were found to terminate under formation of $^1O_2$, whereas for NaO_2 only 1.68% of the trajectories ended up in $^1O_2$ formation. This represents an inverse trend to that reported in the literature. This observation suggests that the dissociation is a viable, monomolecular reaction path to $^1O_2$ that complements the disproportionation pathway.

1. Introduction

1.1. Metal/Air-Batteries and the Pathways to Singlet Oxygen

The reactivity of reduced oxygen species (ROS) in alkali-metal/air battery systems or more specifically in aprotic alkaline metal/oxygen-batteries (AAOBs), most often discussed in terms of lithium- and sodium air-batteries, is one of the major challenges in realizing these promising systems.[1–10] By combining a metal anode with an oxygen gas cathode, unprecedented theoretical energy densities of 11429 $Whkg^{-1}$ and 2646 $Whkg^{-1}$ for Li- and Na-AAOBs, respectively have been postulated.[2,11,12] However, the underlying redox chemistry is hampered by parasitic side reactions that irreversibly damage electrochemically essential cell materials[13–15] and continuously degrade additive cell components such as redox-mediators.[16,17] The reaction with electron-rich reduced oxygen species produces side-products, e.g. Li_2CO_3[18,19] or LiOH.[20–22] Since the influence of these components disrupts the functionality of the metal/air-cell, the question of the mechanism of their formation has received considerable attention.[15,23,24]

Central to the various reaction pathways of parasitic chemistry in metal/air-systems is the formation of singlet oxygen. Singlet oxygen $^1O_2$ is characterized by a higher reactivity with other chemical compounds of the same spin-state compared to the naturally abundant triplet oxygen $^3O_2$.[25,26] Interest in the relationship between singlet and triplet oxygen has been sparked, particularly in relation to reactions with organic compounds. Research into the lifetime of oxygen states and their transitions has led to the development of excitation and deactivation strategies. Studies have also been conducted on environmental chemical effects and photonic excitation.[27–32] In the context of battery systems, singlet oxygen was initially identified in experimental studies by Wandt et al. *in operando*,[33] and its detrimental effect on cell materials was subsequently proposed in a number of studies and literature reviews, highlighting its involvement in a continual degradation of cell components.[24,34,35] It should be mentioned that the possibility of *in operando* $^1O_2$-formation within AAOBs is not undisputed, and the need for further analytical-chemical investigation of ROS formation has been emphasized, e.g., by Schürmann et al.[24] The fundamental mechanistic interpretation of the underlying electrochemistry

[a] D. S. Pietruschka, A. Zaichenko, D. Mollenhauer
Physikalisch-Chemisches Institut, Justus-Liebig-Universität Gießen, Heinrich-Buff-Ring 17, Gießen, D-35392, Germany
E-mail: Doreen.Mollenhauer@phys.chemie.uni-giessen.de

[b] D. S. Pietruschka, A. Zaichenko, D. Mollenhauer
Center for Materials Research (LaMa), Justus-Liebig-Universität, Heinrich-Buff-Ring 16, Gießen 35392, Germany

[c] M. Richter
DS Deutschland GmbH, Am Kabellager 11–13, 51063 Cologne, Germany

[d] S. Gräfe
Institut für Physikalische Chemie and Abbe Center of Photonics, Friedrich-Schiller-Universität Jena, Lessingstr. 4, Jena 07743, Germany

Supporting information for this article is available on the WWW under https://doi.org/10.1002/cphc.202400216

focuses on two questions: First, how is this parasitic species formed during the charge/discharge-process? And second, how can this formation be prevented or mitigated? In the research works of Mahne et al.,[15] Petit et al.[26] and Mourad et al.,[27] the alkaline metal superoxides LiO_2 and NaO_2 have been proposed as key components in the mechanistic pathways. These intermediate species are characterised by their tendency to disproportionate to the corresponding peroxide. Their models of the alkaline superoxide disproportionation reaction and its thermodynamics was based on the hexaatomic molecular dimer structures Li_2O_4 proposed by Bryantsev et al.[36,37] Their research highlighted the complementary nature of weak Lewis acids, such as ammonium cations, present in the solvent as a factor contributing to the distinction between the alkaline homologues.[38] The amount of singlet oxygen $^1O_2$ formed was shown to increase from lithium to sodium-based materials, which was subsequently attributed to the relative size of the energy barriers along the disproportionation mechanism by Petit et al.[26] The involvement of the excited $^1O_2$ state and its relationship to the thermodynamics of the ground state, which changes over the course of the reaction, presents a valuable insight of this study.[27]

Recently, in the theoretical work by Zaichenko et al., an alternative, dissociative pathway leading to the formation of $^1O_2$ has been suggested as a viable alternative mechanism to the disproportionation.[39] In that work, having chosen a small size model system, the dissociation curves of alkaline superoxides could be reliably described using the multiconfigurational CASSCF/CASPT2 methods. The molecular models of superoxides used in that study, i.e. the triatomic LiO_2 or NaO_2, represent the smallest molecular unit capable of achieving the elemental reactivity of dissociation into its constituents. The size of the molecular model used allowed investigating the underlying electronic transition phenomena. Several crossing regions along the calculated potential energy curves with the excited states corresponding to the formation of singlet-oxygen in the $^1\Delta_g$ spin-configuration were found. The relevant important dissociation curves of molecular LiO_2 (Figure 1a) and NaO_2 (Figure 1b) are shown together in Figure 1. Four different crossing points (CP) have been identified and are labelled CP_α to CP_δ for later reference.

In addition to the irreducible representations according to the C_{2v} group, a second labelling scheme is introduced, also because the trajectories were calculated without implying symmetry restrictions. The states are considered in their energetic order for the ground state geometric structre of the superoxide molecule. According to their electronic character, the two lowest states, ascending in energy during dissociation are named as'Ionic 1' (irred. rep. 1^2A_2, lowest curve in black) and 'Ionic 2' (irred. rep. 1^2B_2, curve in red). Here, the metal subunit is present in an oxidized form after transferring one electron to the O_2, reducing it to its superoxide form. These states are abbreviated as I1 and I2, respectively. Conversely, the three states energy-decreasing states during dissociation are referred to as 'Neutral 1' (irred. rep. 1^2B_1, curve in light green),'Neutral 2' (irred. rep. 1^2B_1, curve in light blue) and 'Neutral 3' (irred. rep. 2^2B_1, curve in dark green). These states correspond to an electron configuration in which the metal and oxygen subunits of the LiO_2 are both electronically uncharged. In these configurations, no electron transfer has taken place from M to O_2. In short, these are denoted as N1 to N3. This scheme provides an intuitive analogy to address deviations from C_{2v} symmetry in the molecular structures. Both alkaline superoxides exhibit a qualitatively similar dissociation behaviour: Following curve I1 in both systems along the reaction coordinate at a distance $r_{(Li\text{-}OO,\perp)} = 2.92$ Å (or 3.18 Å in the case of NaO_2), the crossing point CP_α into curve N1 is

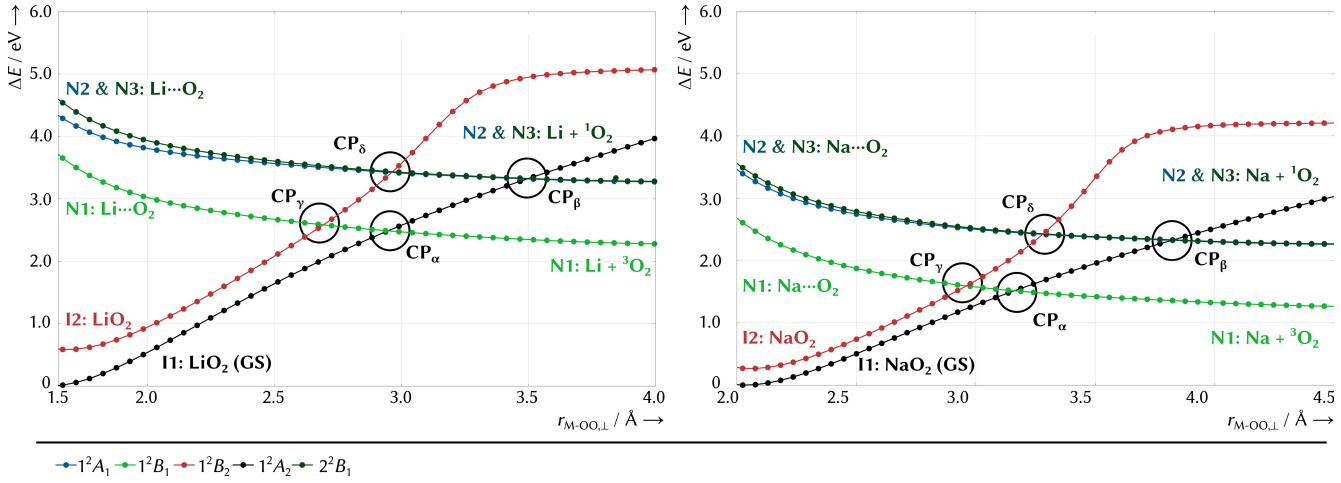

Figure 1. Potential energy curves for the dissociation of the superoxides LiO_2 and NaO_2, calculated at the CASSCF(13,12)/CASPT2/aug-cc-pV5Z level of theory, taken from Ref. [39]. The energy relative to the ground state is plotted against the perpendicular intramolecular distance $r_{M\text{-}OO}$. The oxygen-bond length $r_{O\text{-}O}$ is linearly interpolated between 1.35 Å (superoxide) and 1.21 Å (dissociated system). The energies are given relative to the energy minimum of the ground state. The states are coloured and labelled according to their irreducible representation in the C_{2v}-point group (see Ref. [39] for details). A characterisation of the electronic states is given. The order in which the states are counted refers to the energetic order at the state of the ground state geometric structure (left hand side of the dissociation curves): The first two energetically ascending states referred to as Ionic 1 and Ionic 2 (I1 and I2); the three descending, dissociative electronic states are labelled Neutral 1 to Neutral 3 (N1 to N3). The four crossing points are also labelled CP_α to CP_δ for later reference.

observed. Assuming the states are coupled, this implies an electron transfer from the superoxide O_2^- anion to the metal-ion M^+ and the formation of triplet oxygen ($^3\Sigma_g^-$). For the LiO_2 and NaO_2 systems this coupling is discussed below. Following the ground state further, the second crossing point CP_β is found at 3.50 Å (or 375 Å in the case of NaO_2), which this time crosses with N2 & N3, indicating the formation of the reactive $^1O_2$-species ($^1\Delta_g$). This specific electronic transition is illustrated in Figure 2 below, which shows a schematic of the electron transition between the frontier orbitals at CP_β. For crossings starting from the electronic ground state I1, the intuitive orbital occupation scheme implies electron transitions from the orbitals of the oxygen component of the LiO_2 back to the metal atom, i.e. its reduction to N2.

These crossing points are energetically separated by 0.9 eV. The main difference between the LiO_2-system and the NaO_2-system is that the NaO_2-system is characterised by a lower dissociation energy ΔE_{dis} (1.80 eV compared to 2.30 eV for LiO_2), and the vertical excitation generally requires less energy compared to the LiO_2 system. The two analogous crossings CP_γ and CP_δ of the first excited state in the Franck-Condon region, I2 into N1 or N2 or the degenerate state N3, represent a similar electronic transition from O_2^- back to M^+ but from the orthogonal π*-orbitals of O_2^- and hence forming singlet oxygen depicted in the right-hand side of Figure 2.

1.2. Hypotheses on the Formation of $^1O_2$ in the SHARC-Approach

From these relationships between the excited states of the superoxides and the formation of $^1O_2$ in the static molecular quantum chemical picture, we hypothesise that, given sufficient energy and appropriate probability for electron hopping, population of the singlet oxygen state can be achieved during the dissociation process. The experimental studies of oxygen formation in AAOBs suggest that the majority of oxygen formed is formed as $^3O_2$ while a small fraction is formed as $^1O_2$.[15] A further sub-hypothesis is that the quantitative differences between the potential energy surfaces (PES) of LiO_2 and NaO_2 lead to differences in the population of the electronic state leading to the formation of singlet oxygen.

In order to investigate these hypotheses, in this work, we consider the molecular superoxide dissociation from a dynamics' perspective in this study. The multiconfigurational nature of the molecular model systems LiO_2 and NaO_2[39] has to be maintained in the approach. In addition, non-adiabatic couplings between the different electronic states have to be taken into account in order to correctly describe electronic transitions. This is realized here using the SHARC-program package (acronym for *Surface Hopping including ARbitrary Couplings*), developed by the González group.[40–43]

This allows the computation of *ab initio* Molecular Dynamics (AIMD) trajectories involving transitions caused by coupling between electronic states by means of a "surface hopping" algorithm, originally formulated by Tully.[44,45] The treatment of an ensemble of trajectories, each of which has the possibility to "hop" to a different electronic state at each time step, approximates the quantum mechanical evolution of the nuclear wave packet motion on various potential energy surfaces. The ability of SHARC to adequately reproduce these quantum dynamics results has been shown for various molecular systems.[46–48] SHARC extends the capabilities of Tully's algorithm to arbitrary couplings, including spin-orbit couplings, by introducing an efficient diagonalisation procedure. For a detailed discussion of the SHARC-algorithm the basic methodology article is recommended.[40]

The basic features of the SHARC-algorithm are explained using the hypothesis of $^1O_2$ formation from the alkaline superoxides as an example. For each the two alkaline superoxides respectively, a trajectory ensemble with certain initial conditions (characterised by nuclear coordinates and the corresponding nuclear momenta) is first generated. At each time-step of the AIMD simulation, the nuclear degrees of

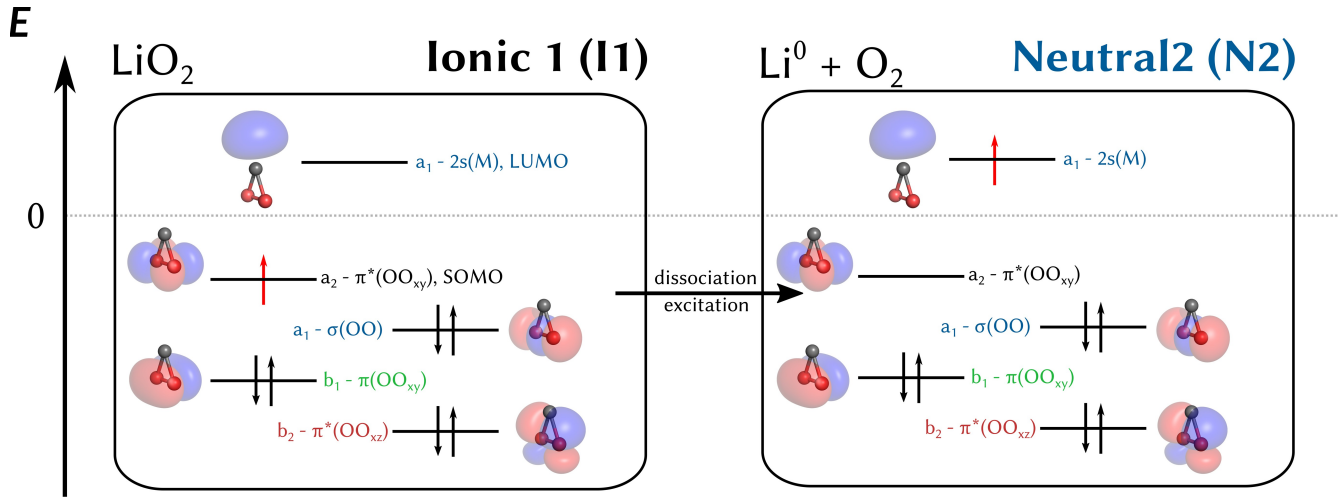

Figure 2. Schematic of the electronic transition from the ground state of LiO_2, $^2A_2$ or I1, into the excited state $^1A_2$ or N2 along CP_β corresponding to the formation of $^1O_2$.

freedom are then propagated along the potential energy surface of the system. The motion of the atoms (e.g. dissociation of the metal atom from the O_2-unit with sufficient energy supply; vibration of the O_2-unit) is calculated classically according to Newton's equations of motion using the (on-the-fly) quantum-chemically computed gradients of the current electronic state. Transition to other states is realised via surface-hopping, based on a probabilistic procedure that takes into account local and non-local (e.g. spin-orbit) couplings. As the coupling terms are highest in the immediate vicinity of the crossing regions, transitions between electronic states will occur predominantly there.[49]

The evaluation of the individual trajectories and the ensemble averages provides an overall expression of the population probabilities and the trajectories' dynamics along the electronic states for given initial conditions. Assignment of the chemical meaning e.g. the distinction between the above-mentioned states N1, N2, I1, I2 and I3 for the alkaline superoxide system is realised by following the localised diabatisation scheme in SHARC. With a sufficiently large number of trajectories, the ensemble mean eventually approaches the behaviour of the natural system. Based on the static picture outlined above, for the state corresponding ultimately to the formation of $^1O_2$, we expect a small number of trajectories to follow this pathway while the majority terminate in the state corresponding to the formation of $^3O_2$.

1.3. Outline of the Presented Study

The present study of SHARC-dynamics begins with an investigation of the MECP employing CASSCF/CASPT2-computations for their search. A full discussion of the influence of the different types of orbitals commonly employed in the multi-configurational post-Hartree-Fock treatment of the system for the computation of the MECP is presented. We show that the commonly used active space restricted to the 2/3*s*-orbitals of the alkali atom and the 2*s*- and 2*p* orbitals of the oxygen atoms, e.g. studies by Allen et al.[50] or Pierini et al.[51] should be extended to include 2/3*p*-orbitals of the alkali metal atom.

Furthermore, the simulation of the dissociating superoxide systems will be presented in detail. We will analyse individual trajectories exemplifying excitation/relaxation patterns. These patterns and the associated reaction channels will be discussed in the context of the static dissociation curves presented by Zaichenko et al.[39] Further, we will compare between the two superoxides, LiO_2 and NaO_2, based on the evaluation of the ensemble averages and the trends observed during the simulation. The discussion of ensemble properties obtained is best expressed through the specific questions "Can singlet oxygen be formed during the dissociation process?" and further "Does the nature of the monomolecular model system lead to quantitative differences in the amount of $^1O_2$ formed?". It also raises the question of whether the observed ratios of $^1O_2$ formation reflect the experimental results. Ultimately, this allows discussion of mitigation strategies and comparison with experimentally observed trends during dissociation and also, as initially presented, during disproportionation.

Computational Details

Search for Minimum Energy Crossing Points

In search for minimum energy crossing points (MECP) between the potential energy surfaces for the dissociation of the LiO_2 and NaO_2 molecules, the optimisation procedures of the *OpenMolcas*-program package were employed.[52,53] As a starting point for the search of these MECPs, the molecular structures of the crossing points provided by Zaichenko et al.[39] were chosen, which are characterised by an intramolecular distance between the alkali atom and the centre of the oxygen bond, $r_{(Li\text{-}OO,\perp)} \approx 2.92$ Å (or 3.18 Å in the case of NaO_2), together with an oxygen-oxygen bond distance $r_{(O\text{-}O)}$ of 1.35 Å.[39] These structures, which represent the points of intersection in the static quantum chemical picture of the linearly interpolated reaction coordinate, were then re-optimised taking into account additional non-geometric constraints. First, only the interatomic distance $r_{(Li\text{-}OO,\perp)}$ together with the bond length of the O_2-unit were taken into account in the optimisation, in order to maintain the fundamental C_{2v} symmetry of the molecules and consequently the irreducible representations of the electronic states. The convergence criterium of difference in their electronic energy at the same coordinates $\Delta E < 10^{-5}$ E_h was required to identify the MECP. The computations were carried out at the SA-CASSCF/CASPT2/cc-pVTZ level of theory.[54,55] The first six doublet states were included with equal weight in the state-averaging.

To assess the influence and composition of the active space on the quality of the description, discussed in detail in the ESI, the computations were carried out employing a (13,12) active space. This active space contains the complete valence electron space including all 2*s* and 2*p* valence orbitals of lithium and oxygen in the case of lithium superoxide and the 3*s*-orbitals and 3*p*-orbitals in the case of NaO_2. Subsequently, the energetically low-lying 2*s*- and 2*s**-oxygen orbitals were considered inactive, i.e. always doubly occupied, and were removed from the active space to form the (9,10) active space. Finally, from this composition of the active-space, the energetically high-lying orbitals with a predominant contribution of the 2*p* orbitals of lithium (or 3*p* orbitals of sodium) were considered secondary, i.e. always unoccupied, and therefore also removed to form a (9,7) active space. This smallest active space - a reduction to only the six 2*p* valence orbitals of the oxygen and a minimal selection of valence orbitals of the reaction partner is employed in literature for example in the quantum chemical modelling of reactive compounds at local minima such as alkaline superoxide dimers[56] or ethylene or vinylene carbonates.[13] In these studies the (9,7) active space was discussed to be sufficient for the structural and energetic characterisation of ground and even transition states of oxygen compounds. For the example of LiO_2, a graphical scheme of the three active spaces is provided in Figure 3.

SHARC-AIMD Studies of the Dissociating LiO_2 and NaO_2

The *OpenMolcas*-program package[52,53] was used by the SHARC-program to calculate the potential energy surface for the trajectories.[31,32] The potential energy surfaces and their gradients at the time steps were calculated at the SA-CASSCF(9,10)/cc-pVTZ[57] level of theory. Six doublet and four quartet states were included in the state-averaging in order to take sufficient account of all electronic states that intersect with each other during the

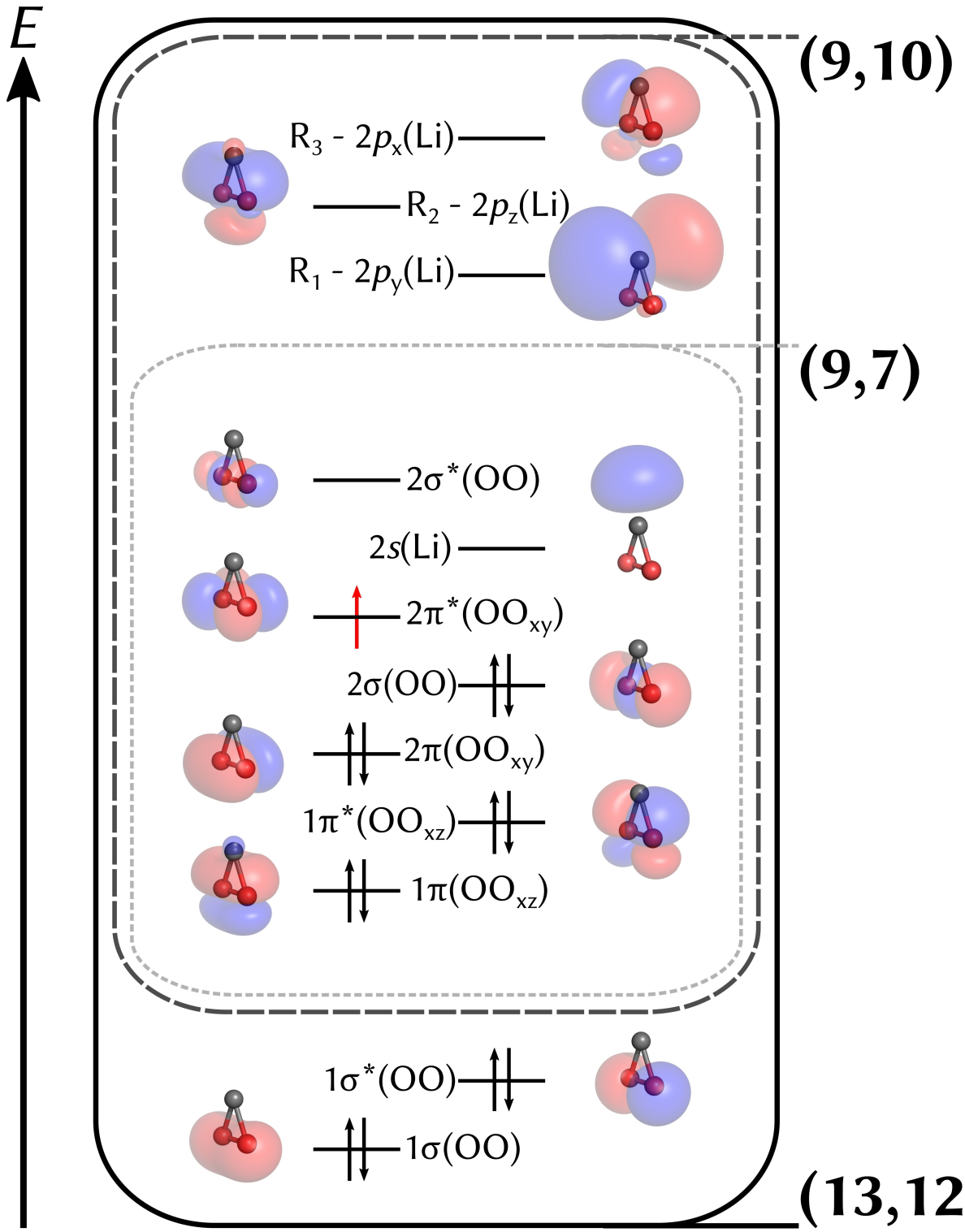

Figure 3. Schematic overview of the three investigated active space sizes studied for the LiO_2-molecule: (13,12) - the full valence space; (9,10) - excluding the 2*s*-orbitals of O_2; (9,7) - excluding the orbitals with predominantly 2*p*(Li) nature. A discussion on the influence of the active space size on the optimisation of the MECP is presented in the ESI.

dissociation process. All states were given equal weight in the state-averaging process. The system was treated without consideration of symmetry to allow for any kind of molecular deformation for the initial starting conditions as well as throughout the simulation runs. Consequently, we apply the alternative naming scheme introduced above. At this level of theory, the analytical computation of gradients was possible, which allowed for sufficient simulation length and an appropriate step size. The ensembles of initial conditions for the SHARC-simulations were first determined by structural optimisation of the electronic

ground state in conjunction with a calculation of vibrational frequencies, which confirmed the obtained structures of LiO_2 and NaO_2 molecules to be local minima. Starting from the ground state nuclear wavefunction, the initial conditions – coordinate pairs and initial momenta – were sampled from a Wigner distribution of a harmonic oscillator model around the ground state minimum.[58,59]

The AIMD simulations were then started from these initial conditions. In a simple modelling approach, the initial conditions for the trajectories were considered in N1, the state corresponding to the 1^2B_1-representation. This vertical excitation was necessary to give the system enough energy to dissociate completely into a single metal atom and a dioxygen unit (see Figure 1). In the case of LiO_2, this state is about 3.5 eV higher in energy than the electronic ground state; for NaO_2 the energy difference is about 2.6 eV. The individual trajectories' total energy remained conserved throughout the simulation; hence, the system can be interpreted as a microcanonical ensemble. A simulation time of 50 fs was considered employing a time step size of 0.5 fs. Hops between all the electronic states, including quartet-electron configurations, are in principle possible. The SHARC-internal local diabatisation and surface hopping scheme was used in conjunction with a decoherence correction developed by Granucci et al.[60]

For LiO_2, 279 trajectories were sampled for the statistical formulation of ensemble averages of the state populations. The number of trajectories was increased to 901 for the NaO_2 system to ensure a sufficient sample size for the formulation of converged ensemble statistics. In all other regards, the statistical evaluation was performed in analogy using the tools of the SHARC program suite. The statistical averages over the entire ensemble were determined by taking into account the sums over the absolute squares of the diabatic coefficients (quantum amplitudes) of each trajectory in the ensemble throughout the simulation. The localised diabatic representation of the trajectories/ensembles was used to correctly correlate the states with their counterparts from the static representation of the dissociation curves and assign their respective chemical meanings.

2. Results and Discussion

2.1. MECPs Along the Dissociation Pathways of LiO_2 and NaO_2

The static picture of the dissociation reaction suggests a central role for the crossing points CP_α and CP_β in possible electronic transition pathways to the electrochemically undesirable $^1O_2$-state. The optimisation and analysis of these crossing points as minimum energy crossing points (MECP) was performed, in particular the states representing the formation of neutral molecular oxygen $^3\Sigma_g^-$ (N1, formed through CP_α) and $^1\Delta_g$ (N2, formed via CP_β). The results of the systems LiO_2 and NaO_2 were compared and contrasted.

Using the MECP optimisation procedure, results were obtained that were consistent with the results of the static linear interpolated intrinsic reaction coordinates (LIIC) dissociation curves (Figure 1). The MECPs are located in spatial regions comparable to the dissociation curve results from Ref. [28]. However, the structures obtained allow the comparison of the internal coordinates outside the limiting linear interpolation approach. Tables 1 and 2 summarise the structural parameters of the four MECP along the dissociation of LiO_2 and NaO_2 optimised at the CASSCF(9,10)/CASPT2/ANO-RCC-TZVP level of theory. The MECPs are labelled according to the scheme introduced in Figure 1, with CP_α and CP_β representing the crossing points from the systems' ground state I1 into the states corresponding to the formation of $^3O_2$ and $^1O_2$, N1 and N2. CP_γ and CP_δ represent analogues of similar electronic transitions starting from the first excited state I2 of the superoxide molecules.

Table 1. Characteristic internal coordinates of the LiO_2 molecule at CP_α to CP_δ, optimised at the CASSCF(9,10)/CASPT2/ANO-RCC-TZVP level of theory considering the system in C_{2v}-symmetry. The labels of the crossing point labels were chosen following the labels in Figure 1. The chemical impact of the crossing points is given in the first column.

MECP	r(M-OO, ⊥)/Å	r(O–O)/Å	ΘO–M-O/°
CP_α ($\rightarrow{}^3O_2$)	2.595	1.230	77.79
CP_β ($\rightarrow{}^1O_2$)	3.095	1.239	78.68
CP_γ ($\rightarrow{}^3O_2$)	2.384	1.234	77.75
CP_δ ($\rightarrow{}^1O_2$)	2.888	1.292	78.04

Table 2. Characteristic internal coordinates of the NaO_2 molecule at the MECP between the lowest states of excitation, optimised at the CASSCF(9,10)/CASPT2/ANO-RCC-TZVP level of theory considering the system in C_{2v}-symmetry. The crossing point labels are chosen in reference to the labels in Figure 1. The chemical significance of the crossing points is given in the first column.

MECP	$r_{(M\text{-}OO,\perp)}$/Å	$r_{(O\text{-}O)}$/Å	$\Theta_{O\text{-}M\text{-}O}$/°
CP_α ($\rightarrow{}^3O_2$)	2.761	1.228	77.80
CP_β ($\rightarrow{}^1O_2$)	3.101	1.232	78.76
CP_γ ($\rightarrow{}^3O_2$)	2.611	1.240	77.68
CP_δ ($\rightarrow{}^1O_2$)	3.054	1.230	79.27

For the crossing points CP_α and CP_β of the LiO_2-molecule, the structural parameters agree very well with those obtained from the calculation with the larger (13,12) active space (shown in Tab. ESI1 and ESI2), and at the same time offer a computationally less demanding option. Most importantly, the succession and order of MECPs along the dissociation coordinate was retained. Hence, the qualitative picture of the static dissociation curves by Zaichenko et al.[28] is conserved in the optimisation procedure. Structurally, the CP are characterised by a large distance between the oxygen atoms and the metal atom and differ from each other in this respect.

An *a priori* exclusion of the M(*p*)-involving orbitals in the optimisation of the MECP [i.e. the choice of a (9,7) active space] was found to distort the picture of an alkali superoxide (see here the ESI for a discussion of these structural distortions). Furthermore, the inclusion of O(2*s*)-orbitals i.e. the choice of a (13,12) active space does not contribute to the spatial or energetic positioning and character of CP_α to CP_β. Quantitative influence was only observed for the later crossing points CP_γ and CP_δ in the case of lithium. These two MECP are of secondary importance to the description of population flow into the states N2 and N3, as will be demonstrated in the following section.

2.2. Dynamic Investigation Using SHARC-AIMD

We now evaluate the possibility of electronic transitions via the CP_α and CP_β and subsequent formation of $^1O_2$ during the dissociation process of LiO_2 and NaO_2. Employing the SHARC simulation protocol, an ensemble of trajectories starting in the state N1 was studied at the SA-CASSCF(9,10)/cc-pVTZ level of theory and analysed using the internal tools of the SHARC program.

The trajectories obtained resembled the shape of the potential energy curves, depicted in Figure 1. The two states I1 i.e., the ground state with crossings CP_α and CP_β and the first excited state I2 with intersections CP_γ and CP_δ increase in energy during dissociation. The states with which they intersect decrease in energy, indicating a transfer of an electron from the superoxide anion back to the metal cation, a reduction of the latter.

Moreover, the parallel progression of the curves between the states N1 and N2 is observed at times of approximately 15 fs onwards of the dissociation. Two excited states (N2 and N3), corresponding to the formation of $^1O_2$ are energetically degenerate, as indicated by the static dissociation curves of Zaichenko et al.[39]

The overview in Figure 4 (vide infra) illustrates a selection of four exemplary dissociation curves, which exhibit remarkable electronic transition processes and features that will be discussed in the following sections. The total energy of the system, which is the sum of its potential and kinetic energy at each time step, is represented by a dotted black line. This energy is conserved throughout the simulation, as indicated by the horizontal line. The states that can be reached from the system's initial total energy via surface hops are presented below the line while those above the line are unavailable due to a lack of energy.

2.2.1. Dissociation of the LiO_2 Molecule

The systematic inspection of all 279 LiO_2 dissociation trajectories revealed that with the chosen SHARC-approach, the dissociation of the superoxide molecules into their components is generally observed in the chosen time window of 50 fs. Due to the initial momenta in the starting conditions, not all trajectories necessarily follow the dissociation pattern resulting from the static dissociation, in which the lithium atom separates itself along a path perpendicular to the

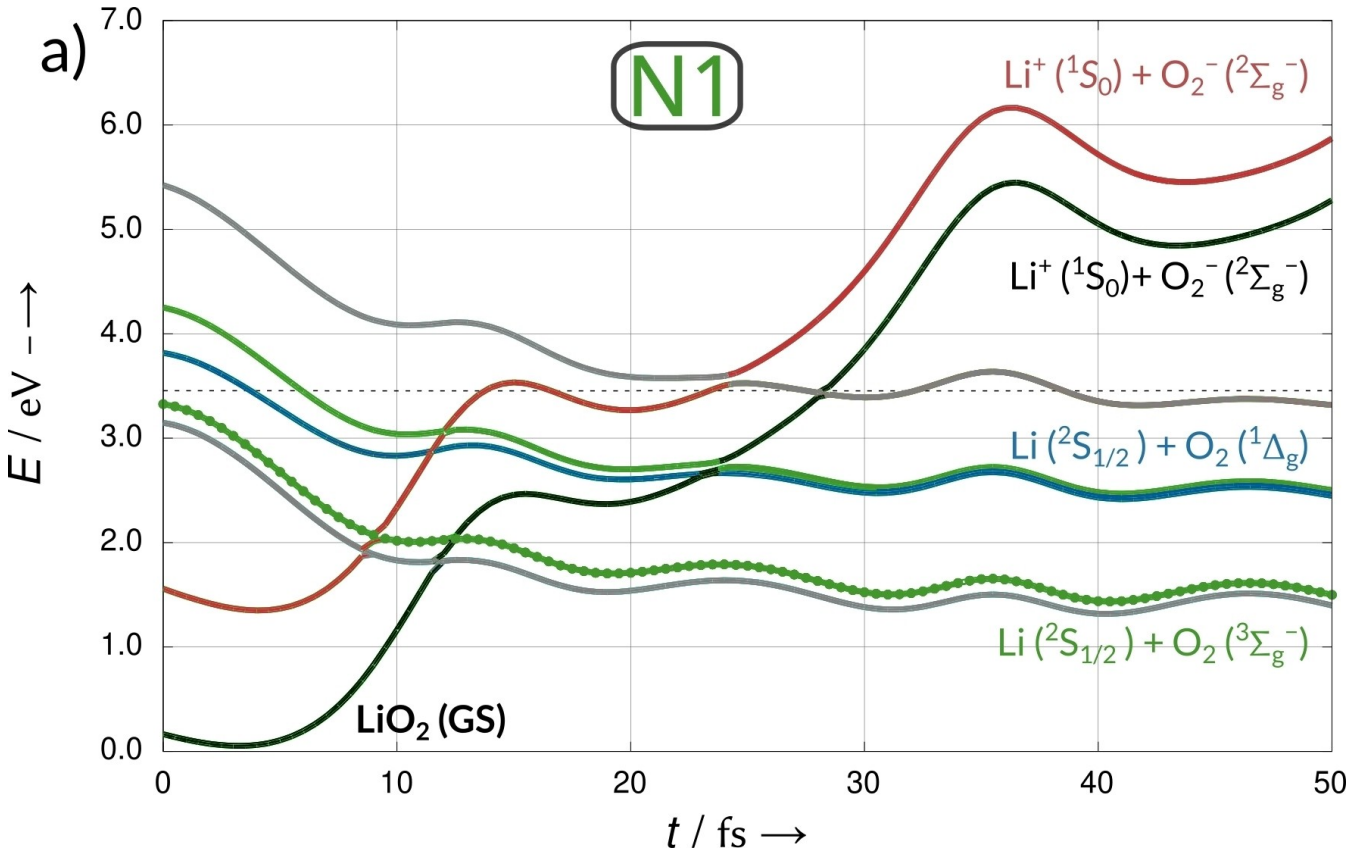

Figure 4. Trajectory of dissociating LiO_2 calculated at the SA-CASSCF(9,10)/cc-pVTZ level of theory. Dissociation of LiO_2 without any electronic transitions from the initial excited state N1. The states are coloured and labelled according to their respective diabatic counterparts in Figure 1. The colours represent the electronic configurations of the following states (in ascending order at $t = 0$): the ionic state I1 (black), ionic state I2 (red), a quartet state that is not populated during the simulation (grey), the neutral state N1 (green, $Li + {}^3O_2$), the neutral states N2 (blue, $Li + {}^1O_2$) and N3 ($Li + {}^1O_2$, green), and another unpopulated quartet state (grey). Term symbols have been added to further clarify the electronic states. The current electronic state on which the dynamics proceeds is signified with a circle on top of a curve in every timestep.

oxygen-bond. The tilt angle $\Theta_{O\text{-}O\text{-}M}$, in some cases up to 25°, notably influences the nature of the dissociation curves by widening the energetic gap between the adiabatic states. This intrinsic connection between geometry and energetic properties was also recently illustrated by Pierini et al.[51] for the dissociating charged LiO_2^--system. This behaviour leads in many cases to avoided crossings along the reaction coordinate.

Along the trajectories of the dissociating systems, surface hops, i.e. electronic transitions between the potential energy surface of the starting state and the energetically ascending states, CP_α and CP_β can be observed in the diagonal representation of the states. In the examples in Figures 4–7, the electronic transitions are predominantly localised near the crossing points, where the energetic difference is lowest and consequentially the coupling terms between two intersecting states are highest.

Examination of all the dissociation trajectories reveals for the LiO_2 system that the vast majority of trajectories follow some dynamics where relaxation into the energetically lowest state in the dissociation limit is observed. This corresponds to the formation of molecular oxygen in the triplet state. In SHARC's diagonal representation of the dissociation curves, this involves relaxation to the ground state in the first 10 to 15 fs, see Figure 4.

The dissociation of the system into its component parts, the direct comparison with the static dissociation picture, presents an oscillation of the energy curves in the energy. This directly corresponds to the continuous oscillation of the oxygen bond. This has little effect on the energetic position of the potential energy curves in relation to each other during dissociation.

The dissociation and electronic excitation of the system into higher states was also observed, as shown in Figure 5. From the initial excitation, the system reaches CP_α with the ascending state I1 as the trajectory progresses. Most of the population enters this state according to the respective contributions of the coefficients after 25 fs, marked by a change in the occupied (dotted) curve.

Finally, this dissociation curve intersects with another excited state. Remarkably, this state N2 (depicted in blue) parallels the ground state by passing through the neutral dissociated state from which neutral Li and $^1O_2$ are produced. This represents an event where dissociation into a state that signifies the formation of singlet oxygen (either N2 or N3) along the intersections is achieved through the MECP. In all

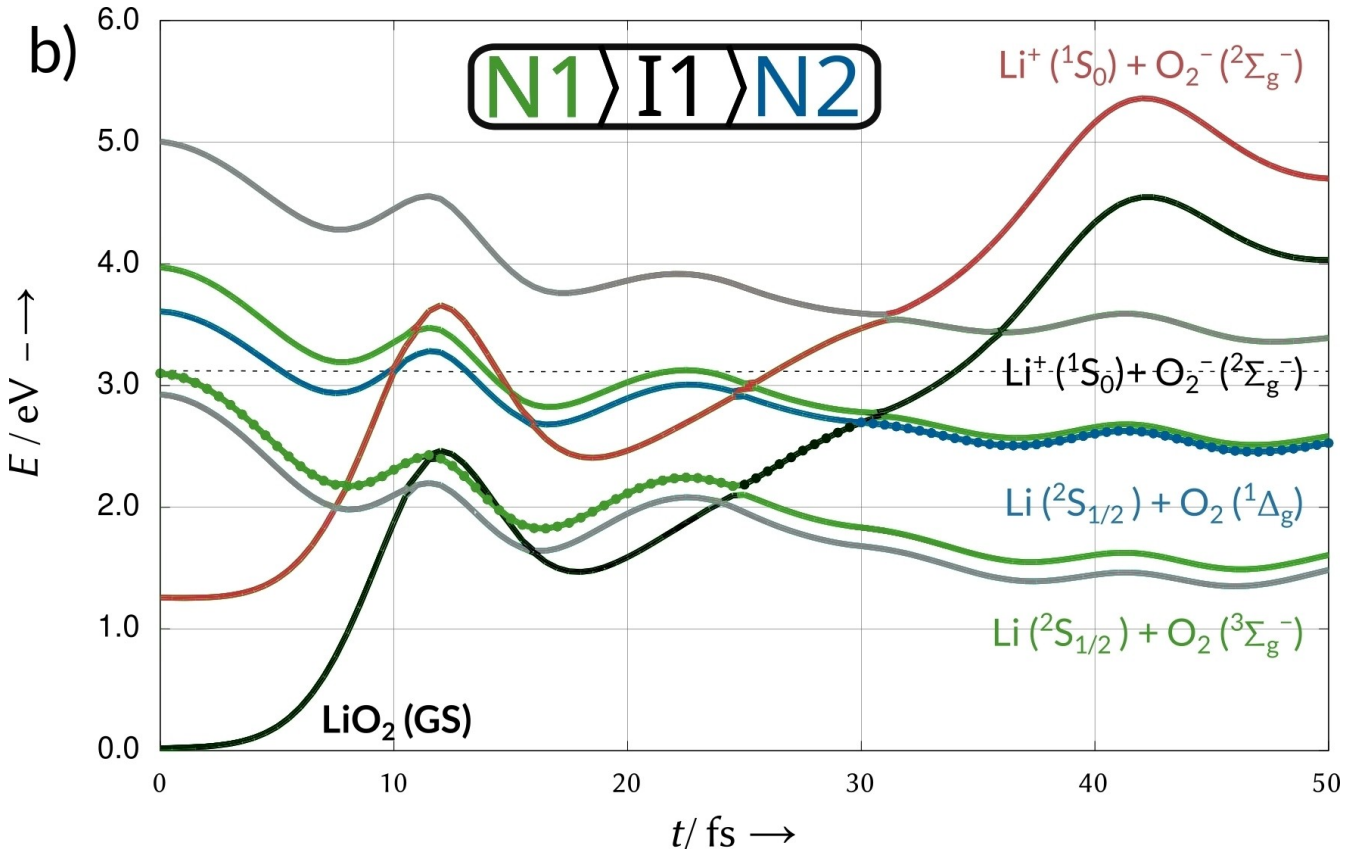

Figure 5. Trajectory of dissociating LiO_2 calculated at the SA-CASSCF(9,10)/cc-pVTZ level of theory. Dissociation of LiO_2 with transition into the state I1 after 25 fs and a second transition to the excited state N2 after 30 fs along CP_β (formation of $^1O_2$.) The states and crossings are coloured and labelled according to their respective diabatic counterparts in Figure 1. The states and crossings in the figure are colour-coded and labelled according to their respective counterparts in Figure 1. The colours represent the electronic configurations of the following states (in ascending order at $t = 0$): the ionic state I1 (black), ionic state I2 (red), a quartet state that is not populated during the simulation (grey), the neutral state N1 (green, $Li + {}^3O_2$), the neutral states N2 (blue, $Li + {}^1O_2$) and N3 ($Li + {}^1O_2$, green), and another unpopulated quartet state (grey). Term symbols have been added to further clarify the electronic states. The current electronic state on which the dynamics proceeds is signified with a circle ontop of a curve in every timestep.

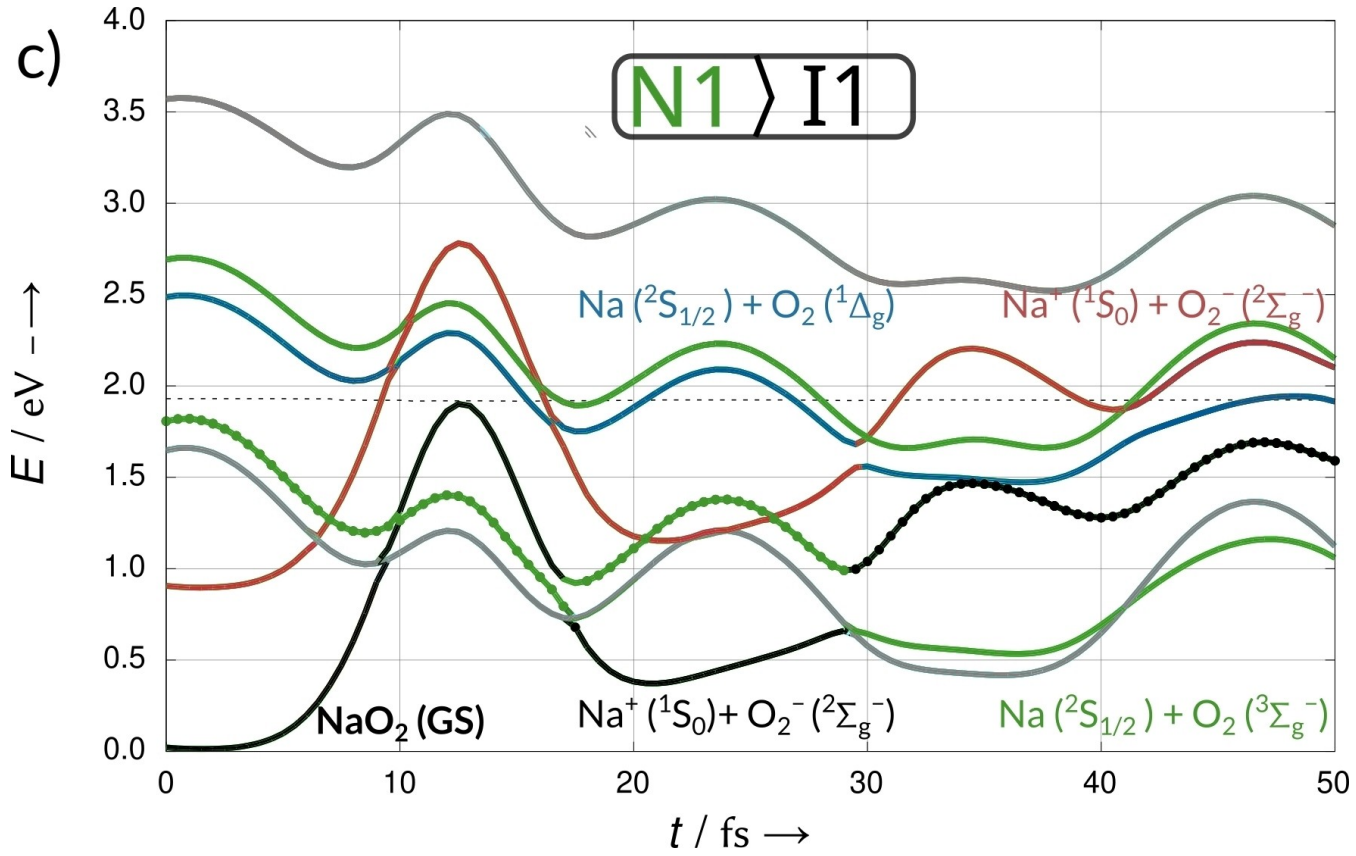

Figure 6. Trajectory of dissociating NaO_2 calculated at the SA-CASSCF(9,10)/cc-pVTZ level of theory. Dissociation of NaO_2 with transition into an excited state I1 along CP_α after 29 fs. The states are coloured and labelled according to their respective diabatic counterparts in Figure 1. The states and crossings are coloured and labelled according to their respective counterparts in Figure 1. The states are coloured and labelled according to their respective counterparts in Figure 1. The colours represent the electronic configurations of the following states (in ascending order at $t=0$): the ionic state I1 (black), ionic state I2 (red), a quartet state that is not populated during the simulation (grey), the neutral state N1 (green, $Na+{}^3O_2$), the neutral states N2 (blue, $Na+{}^1O_2$) and N3 ($Na+{}^1O_2$, green), and another unpopulated quartet state (grey). Term symbols have been added to further clarify the electronic states. The current electronic state on which the dynamics proceeds is signified with a dot in every timestep.

trajectories, N2 and N3 exhibit a characteristic energy difference of 0.9 eV relative to the ground state N1. This energy gap indicates the electronic state of a neutral metal atom (Li/Na) both ground and excited state and triplet oxygen ($^3O_2$) for the ground state curve N1 and singlet oxygen ($^1O_2$) for the degenerate excited state curves (N2 and N3). This value agrees with the ones previously obtained by Zaichenko at the CASSCF(13,12)/CASPT2/cc-pV5Z level of theory (see Figure 1). It should be noted that this event, together with the transition into the energetically degenerate state N3 (depicted in dark green), is observed less frequently but still significantly in the 279 trajectories (see Table 3 in section 3.3).

It is observed that the trajectories entering via CP_α and remaining in the ascending excited state I1 (depicted in black) begin to return to the initial ground state after about 20 to 25 fs. Interestingly, these states introduce a degree of reversibility into the observation of the dissociating molecule: In some rare cases, they are observed to decay largely, but not completely, and in the final frames of the simulation, the dissociation of the molecule appears to reverse. This behaviour can be interpreted as an internal relaxation pathway open to the excited superoxide species.

Table 3. Population probabilities $P(MO_2)$ for the five lowest doublet-states of LiO_2 (279 trajectories) and NaO_2 (901 trajectories) at the end point ($t=$ 50 fs) of the simulation run. The SHARC trajectories were calculated without symmetry.

Electronic state	$P(LiO_2)$/%	$P(NaO_2)$/%
I1 ($MO_2 \rightarrow M^+ + O_2^-$)	7.65	10.73
I2 ($MO_2 \rightarrow M^+ + O_2^-$)	0.00	0.00
N1 ($MO_2 \rightarrow M + {}^3O_2$)	85.13	87.58
N2 ($MO_2 \rightarrow M + {}^1O_2$)	**0.33**	0.00
N3 ($MO_2 \rightarrow M + {}^1O_2$)	**6.52**	**1.68**

Finally, the coefficients of the quartet-states (shown in a grey tone in Figures 4–7) indicate that spin-crossings into these states are observed at a rate three to four orders of magnitude lower than into the doublet-states outlined. We conclude that these types of crossing are of no practical importance in the dynamical studies of the model systems presented. It suggests that these states are not relevant to battery processes unless specifically affected by the introduction of heavy atoms in the chemical environment.

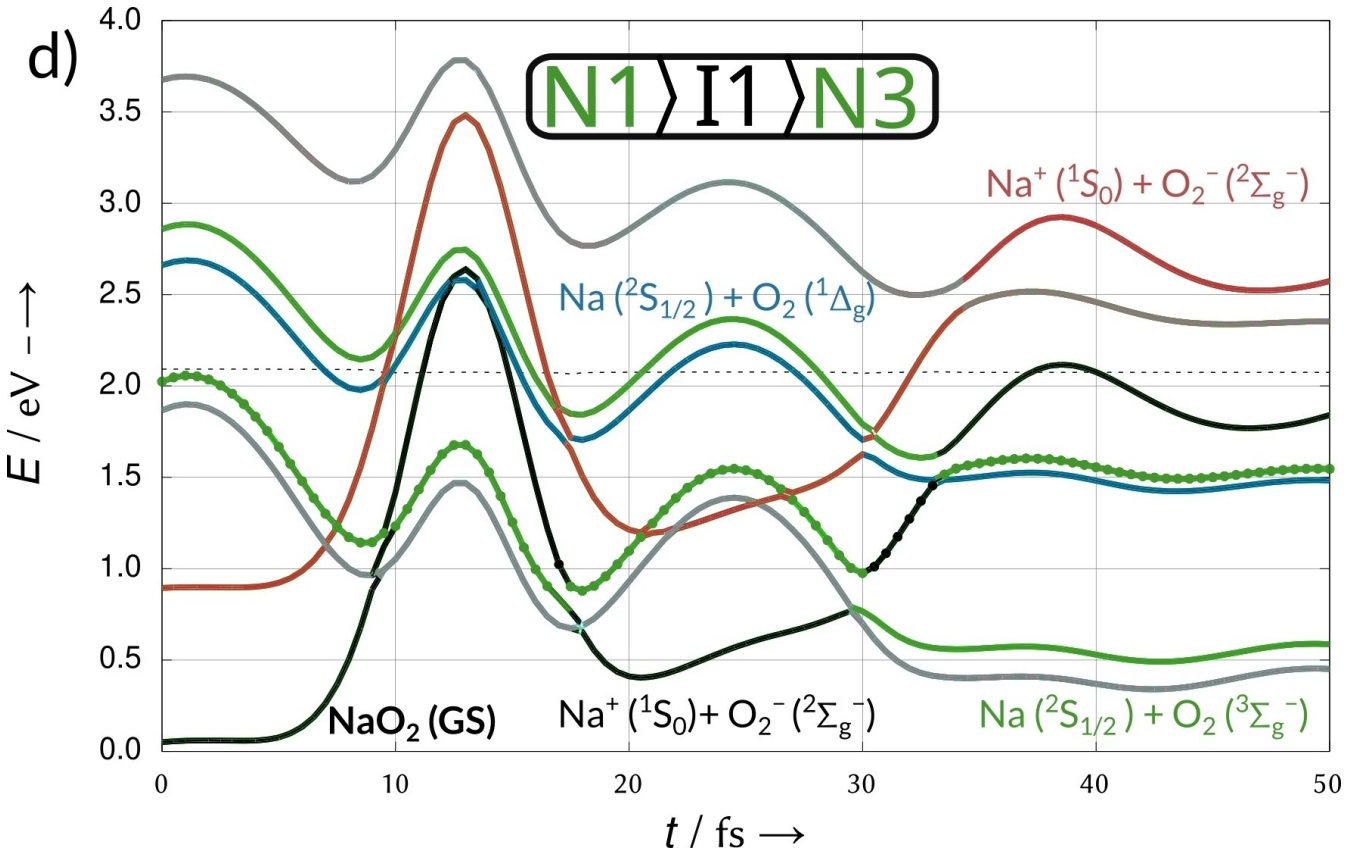

Figure 7. Trajectory of dissociating NaO_2, calculated at the SA-CASSCF(9,10)/cc-pVTZ level of theory. Dissociation of NaO_2 with a first transition into the state I1 along CP_α state after 30 fs and a second transition into N3 a further excited state along CP_β (formation of $^1O_2$). The states are coloured and labelled according to their respective diabatic counterparts in Figure 1. The states and crossings are coloured and labelled according to their respective counterparts in Figure 1. The states are coloured and labelled according to their respective counterparts in Figure 1. The colours represent the electronic configurations of the following states (in ascending order at $t=0$): the ionic state I1 (black), ionic state I2 (red), a quartet state that is not populated during the simulation (grey), the neutral state N1 (green, $Na+{}^3O_2$), the neutral states N2 (blue, $Na+{}^1O_2$) and N3 ($Na+{}^1O_2$, green), and another unpopulated quartet state (grey). Term symbols have been added to further clarify the electronic states. The current electronic state on which the dynamics proceeds is signified with a dot in every timestep.

2.2.2. Dissociation of the NaO_2 Molecule

In analogy to the LiO_2 molecule, the NaO_2 molecular system dissociates in a manner that can be deduced from the PESs by Zaichenko et al.[39] Two exemplary energy-time curves are shown in Figures 6 and 7. The same energetic sequence of states along the dissociation pathway is observed as in Figure 1, including the crucial MECP CP_α and CP_β. The first leads to a crossing into the state N1 representing the formation of triplet-oxygen $^3O_2$. This is followed by the formation of singlet-oxygen $^1O_2$, further along the intrinsic reaction coordinate through the states N2 or N3. The most notable difference from the LiO_2 dissociation curves is a generally lower potential energy at the beginning of the trajectories. While for LiO_2, the initial conditions sampled from the Wigner-distribution characterize a total energy between 3.0 and 3.5 eV, for NaO_2 the total energy ranges between 1.7 and 2.3 eV. This is again consistent with the static picture of the dissociation.

For NaO_2, analogous to the dissociation of LiO_2, the system separates into two components over time, although the motion of dissociation proceeds slower by a factor of three due to the heavier mass of sodium. As shown in Figures 6 and 7, electronic transitions to higher states N2 and N3 are also observed at later times, after about 30 to 35 fs. Characteristic transition pattern between states, as described in the previous sections, were observed throughout the ensemble of trajectories, albeit at a lower rate. Most of the trajectories followed a transition-less dissociation pathway into the electronic ground state in the dissociation limit, corresponding to the formation of a sodium atom and triplet oxygen $^3O_2$. To test for the possibility that the sample size was insufficient to represent the dynamics, the total number of trajectories was increased to 901. This test showed that the average probability of an electronic transition occurring in the states associated with the formation of $^1O_2$ is indeed lower.

An example of the population of the transition to one of the two degenerate excitations N2 or N3 corresponding to the formation of $^1O_2$ is shown in Figure 7. After 30 fs, a transition to the ascending state I1 (coloured in black) and finally to the $^1O_2$-signifying state N2 or N3 is observed. The slow movement of the sodium-atom/ion ensures that relaxation to the ground

state in this trajectory is prevented and instead the trajectory assumes the excited state N2 during dissociation. It should be noted that for this selected trajectory, an initial inclination of $\Theta_{O\text{-}O\text{-}M}$ as approximately 18° is observed, again highlighting the importance of this structural parameter identified by Pierini et al.[51]

A final class of trajectories is presented in Figure 6 where the trajectories exhibit the formerly identified internal relaxation pattern. These trajectories occurred at a higher rate than the electronic transition to singlet oxygen. While the general trend is towards complete dissociation of the system, there are exceptions: In the final steps of some trajectories of the simulation, the dissociation process starts to reverse due to insufficient momentum against the slope of the potential energy surface. Hence, beside the nature of the PES, the initial conditions of the simulation determine this behaviour. This behaviour of the system follows this internal relaxation mechanism into the ground state I1 from the initial vertical excitation into N1.

One last point to mention: Although the total energy differs between the two molecules LiO_2 and NaO_2, the gradients are similar in both cases.

2.3. Analyses of the Trajectory Ensembles

Beyond the evaluation of the individual trajectories, the analysis of ensembles helps to quantify and extend the previous observations. From the individual trajectories, we show that for both dissociating superoxides, the formation of $^1O_2$ is observed as a rare event. To study the evolution of the population, the sum of the quantum amplitudes and their change with time are considered. Normalisation to the number of trajectories then allows for a probabilistic interpretation. The normalised probability-time-plots for both systems are presented in Figure 8. This visualisation is accompanied by a tabular overview of the final population, presented in Table 3.

The analysis of the ensemble's population probability across the five lowest doublet states of the system and over time complements the discussion of individual trajectories. For both LiO_2 and NaO_2, an onset of population flow along the intersection CP_α into the state I1 is observed after approximately 15 fs. For LiO_2, a larger fraction of the trajectories, about 19% at a given time, follow this path. For NaO_2 about 8% of the trajectories exhibit this dissociation pattern. This population increases until, for LiO_2 at approximately 28 fs and for NaO_2 at about 31 fs, new channels of electronic transition open up to the system. At this point, the population begins to flow into the states corresponding to singlet oxygen, N2 and N3 with one of the two degenerate states, N3, being populated favourably. Both, the excited states signifying the reduction under formation of $^1O_2$ (along CP_β), as well as the states corresponding to the formation of a metal cation and superoxide anion, I1 (along CP_α), are very sparsely populated at all points in the simulation. A second type of trajectory behaviour is observed in the slow return to population of the initial ground state I1 of the alkaline superoxides. This behaviour indicates that a certain number of the trajectories do not complete the dissociation, but instead an inversion of the reaction coordinate i.e. a relaxation of the system from initial N1 into ground state I1 is observed.

While for LiO_2 the combined probability of systems exhibiting the electronic configuration of singlet oxygen and a neutral lithium atom in a dissociated state, N2 and N3 amounts to approximately 6.85%, for NaO_2 a lower probability of 1.68% for the $^1O_2$ formation was observed. The vast majority of trajectories remained in the electronic state corresponding to the formation of triplet oxygen. It is noteworthy that in the case of LiO_2 7.65% and in the case of NaO_2 10.73% occupy the intermediate ionic state from which relaxation to the ground state is possible.

Comparison of these results to experimental findings and recent mechanistic studies demonstrates that the reaction channel toward the formation of singlet oxygen is available alongside the predominant channel leading to the formation of triplet oxygen. Under the condition of an initial energy supply, as is conceivable e.g., under the influence of the Ohmic drop or by the application of an external potential in the charging process, this represents an available monomolecular pathway to the formation of oxygen species in both

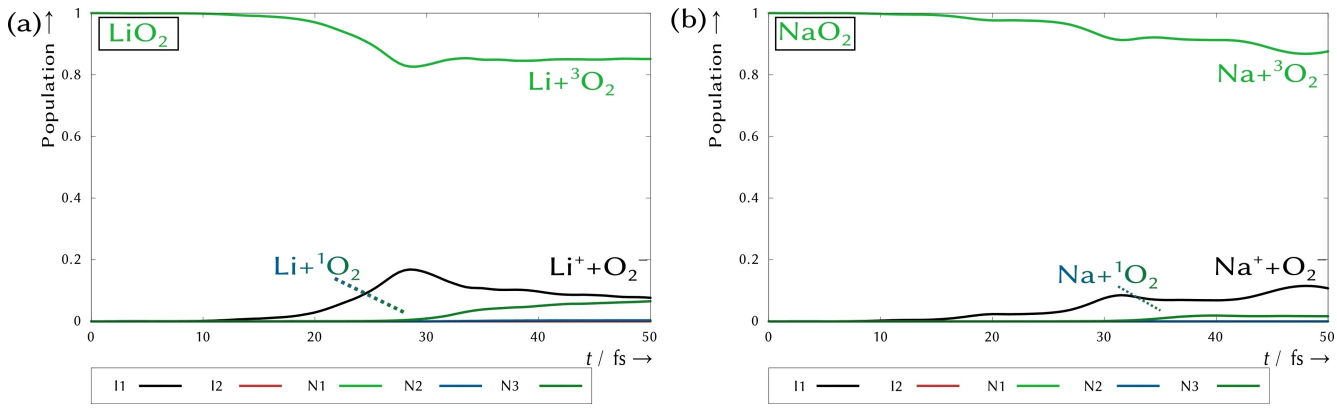

Figure 8. Temporal progression of the normalised populations of the five energetically lowest doublet states of LiO_2, obtained from the analysis of the quantum amplitudes of 279 SHARC dissociation trajectories and of NaO_2, obtained from the analysis of the quantum amplitudes of 901 SHARC-dissociation trajectories. The naming and colour scheme is chosen in analogy to the labels presented in Figure 1, I1 and I2, N1 to N3.

spin configurations. Furthermore, as was demonstrated in addition, based on the difference of the atomic mass of the alkali metal atoms, a trend in the reactivity of the alkaline systems could be established: For a slower change in the systems nuclear coordinates, a lower transition probability is expected according to the adiabatic theorem.[61] Finally, the reaction channel to singlet oxygen is less populated for NaO_2 than for LiO_2. Following the same trends, a smaller fraction of the singlet oxygen ($^1\Delta_g$) is expected to be formed during dissociation of superoxides such as KO_2. Furthermore, transitions via the quartet states are considered to play a more central role for this system.

This observation contrasts with the results of the Freunberger group on the disproportionation behaviour of the alkaline superoxides LiO_2 and NaO_2.[26,27] They provided a mechanistic study of patterns describing the reactivity in the alkali/air-systems, based on the chemical synthesis of superoxide combined with a density functional theory-based approach. By stabilisation of the peroxidic species, it was possible to increase the propensity of the system to the disproportionation mechanism and consequently to the formation of molecular oxygen. Additionally, the introduction of weak Lewis acids was shown to increase the ratio of singlet oxygen to triplet oxygen in the mixture of O_2 formed during the reaction.

The disproportionation of LiO_2 and NaO_2 in a tetraethylene glycol dimethyl ether solution (TEGDME) was expected to result in a small fraction of the oxygen formed having a singlet spin-configuration. Approximately 2% of the oxygen from the disproportionation of LiO_2 and up to 12% of the oxygen from the NaO_2 were proposed by the authors to be $^1O_2$. This is the opposite trend compared to the ratio determined for the amount of singlet-oxygen formed during the SHARC-AIMD dissociation dynamics. It must be mentioned, however, that this interpretation of the experimental findings is not unanimously agreed upon. Schürmann et al. have raised a critique on the basis of stability windows for the lithium superoxides and peroxides within the AAOBs.[34]

We believe that the results indicate that the presented mechanistic pathway of singlet oxygen formation by dissociation complements rather than contradicts the interpretation of Mourad et al. who suggest disproportionation as the main cause.[56,62] It is advisable to interpret it as an alternative reaction channel, which in particular has the inverse property of being more open in the case of LiO_2 and requiring only one superoxide monomer. The consideration that there are multiple mechanistically unique channels for the formation of singlet oxygen was also recently proposed by Dong et al.[63] They observed a bond cleavage channel responsible for more than 40% of the $^1O_2$ formed during the disproportionation. In the light of these results, the evaluation of the elemental reaction step of the dissociation as an additional pathway is highly relevant, especially when considered in the context of trying to reduce or avoid the formation of $^1O_2$ under operating conditions within metal/air-battery systems. A direct investigation of the MO_2-dimer systems' excited state dynamics via SHARC is currently not feasible due to the exponential increase in computational demand resulting from the necessary increase of the active space. The consistent size of a (9,10) active space allowed for the first quantitative analysis of the population flow during the dissociation process. With regards to the disproportionation of two MO_2, it may be necessary to consider increasing the active space to either (18,20) active space (medium active space size) or (18,14) active space (small size). Additionally, the elementary step of dissociation is not straightforward for these systems due to the increased number of potential degrees of freedom among the hexaatomic systems as compared to the triatomic monomers. For the dissociation mechanism, this task translates directly into the question of how crossings between the ascending ground state and the states leading to the formation of $^1O_2$ in the dissociation limit can be avoided.

The introduction of an extended atomic environment in the form of a support or solvent offers a direct way to shift the relative energetic position of the potential energy surfaces with respect to each other.[39] In particular, the distinction between ionic and neutral states can allow for specific tuning of the energetic gaps and positioning of the crossing points. This is currently subject of further investigation on the class of the alkaline oxygen compounds of different oxidation states and embedded in chemical environments. There is also the question of whether the mechanism of disproportionation exists also exhibits MECP between coupled states in a dissociative elementary reaction step. And if so, how might a step involving cleavage of the O_2-bond incorporate it? This is a particular important subject of discussion when dissociative elementary steps are proposed, e.g., in the primary mechanistic studies of LiO_2 disproportionation by Bryantsev et al.[51]

Finally, the limitations of the approach presented here for assessing population fluxes during disproportionation behaviour are considered. In order to provide the system with sufficient energy for the dissociation, a vertical excitation into its second excited doublet state was chosen. Sufficient energy supply within chemical cells can be achieved by the Ohmic drop at the electron interface.[50] Additionally, the groundbreaking research of Nørskov et al.[64] demonstrated that the energetic position of reactants experiences a bias potential shift relative to the reaction products, which is directly proportional to an applied bias potential U_{bias}. This shift could potentially widen the distance between or even prevent the crucial motif of MECP in the potential energy landscape of the dissociation step leading to the formation of $^1O_2$. The presence of the intermediate superoxide species in these regions is achieved during operation of the cell in both the discharge as well as the charging procedure, where the application of U_{bias} plays a critical role.[24] Moreover, this vertical excitation process does not necessarily have to be representative of battery phenomena. In all cases where singlet oxygen was formed, the population passed through the state corresponding to the electronic ground state, I1. Therefore, we assume that different types of energy absorption generally represent the results discussed. In this approach, successful dissociation curves and the localisation of electronic transition near the MECPs were observed.

The triatomic superoxide model system used represents the smallest possible molecularly reactive chemical representation of the superoxide intermediates. This model system size allowed the SHARC-AIMD-study to be treated using the multiconfigurational method CASSCF for an accurate description of the different excited states. Due to these model assumptions, the scope of this study is necessarily limited to the possibility of $^1O_2$-formation in the monomolecular reaction. However, it is shown that this mechanistic route allows the generalisation of this reaction pattern to other, broader chemical reactions in batteries. A complex embedding matrix of the system can then be interpreted as a perturbation of this basic reaction pattern. Hence, the dissociative elementary step leading to the formation of molecular oxygen always needs to be investigated to facilitate the population of excited state channels, ultimately forming $^1O_2$.

3. Conclusions

In this study, the mechanism of dissociation of superoxide molecules as a possible source of reactive singlet-oxygen $^1O_2$ in the context of metal/air-battery was investigated using theoretical methods. Based on the research of Zaichenko et al.,[39] the question was investigated whether minimum energy crossing points between electronic states corresponding to the formation of singlet oxygen are a reason for the formation of this species. It was also investigated how differences between the alkaline superoxides LiO_2 and NaO_2 translate into different rates for the reactive oxygen species formation.

For this purpose, an optimisation of the MECP along the reaction coordinate demonstrates qualitative agreement of the static picture of the dissociation initially proposed in the work of Zaichenko et al.[28] Three different active spaces were studied. Quantitatively similar structures and energies were obtained between the (13,12) and the (9,10) active spaces, and, for the most part, the (9,7) active space. However, it was found that optimisation of important MECP between the ground state and the excited state corresponding to the formation of reactive singlet-oxygen, e.g., the CP_β gave incorrect structural parameters for the smallest (9,7) active space.

Building on the static description of the dissociation reaction and the identified MECPs, the SHARC-AIMD approach was used to model the population of the states corresponding to the formation of $^1O_2$ in a dynamics approach. The individual trajectories and the quantum amplitudes of the trajectory ensembles illustrate a complete dissociation characterised by rare but still realized reaction channels into the electronic configuration of singlet oxygen. The trajectories, which eventually populate the singlet-oxygen states show characteristic excitation patterns. We consider the presence of these patterns as a potential indicator for the possibility of $^1O_2$-formation in reactions with a comparable elementary step in which an oxygen unit dissociates from an electron transfer partner.

Differences in the rate of the dissociation reaction were observed to influence the extent to which the non-adiabatic transition to these excited-state configurations were observed. For example, the probability of LiO_2 forming $^1O_2$ during dissociation is 6.85 % whereas for the heavier NaO_2 molecule it is approximately 1.68 %.

The ab initio molecular dynamics simulations using high-accuracy multiconfigurational post-Hartree-Fock methods approach provides fundamental insights into the elementary steps of an intermediate reactivity in metal/air-batteries. In the context of recent mechanistic studies of $^1O_2$-formation in alkaline metal/air-cells, these results show an inverse trend to documented findings, presenting a complementary reaction channel. In the discussion of how to mitigate the formation of singlet-oxygen, the importance of an appropriate solvation approach is emphasised, and further investigations are required to embed the elementary dissociative reaction step in an extended environment. Future discussion should also extend to the introduction of possible additives to the system such as quenching agent. The results presented demonstrate the importance of excited state phenomena in the discussion of chemical reactivity within metal/air-systems and batteries.

Acknowledgements

The authors wish to thank the "Deutsche Forschungsgesellschaft (DFG)-Graduiertenkolleg" (GRK 2204) for its financial support.

Furthermore, they wish to express thanks for the support by the administrators of the *YACANA*-cluster of the Justus-Liebig Universität, Gießen. The authors would also like to thank the *Hessian Competence Center for High Performance Computing/* (HKHLR) – funded by the *Hessen State ministry of Higher Education, Research and Arts* – for helpful advice. S.G. would like to highly acknowledge funding from the DFG via the Research unit "FuncHeal", project ID 455748945-FOR 5301 (project P5). Open Access funding enabled and organized by Projekt DEAL.

Conflict of Interests

The authors declare no conflict of interest.

Data Availability Statement

The data that support the findings of this study are available in the supplementary material of this article.

Keywords: Post-Hartree-Fock-methods · Surface-hopping dynamics · Metal/air batteries · Singlet-oxygen

[1] D. Geng, N. Ding, T. S. A. Hor, S. W. Chien, Z. Liu, D. Wuu, X. Sun, Y. Zong, *Adv. Energy Mater.* **2016**, *6* (9), 1502164. https://doi.org/10.1002/aenm.201502164.

[2] W.-J. Kwak, D.S. Rosy, C. Xia, H. Kim, L. R. Johnson, P. G. Bruce, L. F. Nazar, Y.-K. Sun, A. A. Frimer, M. Noked, S. A. Freunberger, D. Aurbach, *Chem. Rev.* **2020**, *120* (14), 6626–6683. https://doi.org/10.1021/acs.chemrev.9b00609.
[3] Q. Liu, Z. Pan, E. Wang, L. An, G. Sun, *Energy Storage Mater.* **2020**, *27*, 478–505, https://doi.org/10.1016/j.ensm.2019.12.011.
[4] Y. Liu, L. Wang, L. Cao, C. Shang, Z. Wang, H. Wang, L. He, J. Yang, H. Cheng, J. Li, Z. Lu, *Mater. Chem. Front.* **2017**, *1* (12), 2495–2510. https://doi.org/10.1039/C7QM00353F.
[5] R. Cao, K. Chen, J. Liu, G. Huang, W. Liu, X. Zhang, *Sci. China Chem.* **2024**, *67* (1), 122–136, https://doi.org/10.1007/s11426-023-1581-2.
[6] M. C. Policano, C. G. Anchieta, T. Carpanedo De Morais Nepel, F. C. B. Maia, R. M. Filho, G. Doubek, *J. Electrochem. Soc.* **2023**, *170* (4), 040522. https://doi.org/10.1149/1945-7111/acc2ea.
[7] L.-N. Song, L.-J. Zheng, X.-X. Wang, D.-C. Kong, Y.-F. Wang, Y. Wang, J.-Y. Wu, Y. Sun, J.-J. Xu, *J. Am. Chem. Soc.* **2024**, *146* (2), 1305–1317. https://doi.org/10.1021/jacs.3c08656.
[8] Y. Ding, Y. Li, Z. Wu, *Battery Energy* **2023**, *2*(2), 20220014. https://doi.org/10.1002/bte2.20220014.
[9] T. Liu, S. Zhao, Q. Xiong, J. Yu, J. Wang, G. Huang, M. Ni, X. Zhang, *Adv. Mater.* **2023**, *35* (20), 2208925. https://doi.org/10.1002/adma.202208925.
[10] S. S. H. Zaidi, X. Li, *Adv. Energy Mater.* **2023**, *13* (28), 2300985. https://doi.org/10.1002/aenm.202300985.
[11] H. Gao, B. M. Gallant, *Nat. Chem. Rev.* **2020**, *4* (11), 566–583. https://doi.org/10.1038/s41570-020-00224-7.
[12] Z. Khan, M. Vagin, X. Crispin, *Adv. Sci.* **2020**, *7* (5), 1902866. https://doi.org/10.1002/advs.201902866.
[13] A. T. S. Freiberg, M. K. Roos, J. Wandt, R. de Vivie-Riedle, H. A. Gasteiger, *J. Phys. Chem. A* **2018**, *122* (45), 8828–8839. https://doi.org/10.1021/acs.jpca.8b08079.
[14] J. W. Mullinax, C. W. Bauschlicher, J. W. Lawson, *J. Phys. Chem. A* **2021**, *125* (14), 2876–2884. https://doi.org/10.1021/acs.jpca.1c00605.
[15] N. Mahne, B. Schafzahl, C. Leypold, M. Leypold, S. Grumm, A. Leitgeb, G. A. Strohmeier, M. Wilkening, O. Fontaine, D. Kramer, C. Slugovc, S. M. Borisov, S. A. Freunberger, *Nat. Energy* **2017**, *2* (5), 17036. https://doi.org/10.1038/nenergy.2017.36.
[16] Y. Dou, Z. Xie, Y. Wei, Z. Peng, Z. Zhou, *Natl. Sci. Rev.* **2022**,*9*, nwac040. https://doi.org/10.1093/nsr/nwac040.
[17] W.-J. Kwak, H. Kim, Y. K. Petit, C. Leypold, T. T. Nguyen, N. Mahne, P. Redfern, L. A. Curtiss, H.-G. Jung, S. M. Borisov, S. A. Freunberger, Y.-K. Sun, *Nat. Commun.* **2019**, *10* (1), 1380. https://doi.org/10.1038/s41467-019–09399-0.
[18] H. Gan, E. S. Takeuchi, *J. Power Sources* **1996**, *62* (1), 45–50. https://doi.org/10.1016/S0378-7753(96)02405-6.
[19] O. Axelsson, Y. Shao, J. Paul, F. M. Hoffmann, *J. Phys. Chem.* **1995**, *99* (18), 7028–7035. https://doi.org/10.1021/j100018a040.
[20] B. E. Deal, H. J. Svec, *J. Am. Chem. Soc.* **1953**, *75* (24), 6173–6175. https://doi.org/10.1021/ja01120a019.
[21] J. Phillips, J. Tanski, *Int. Mater. Rev.* **2005**, *50* (5), 265–286. https://doi.org/10.1179/174328005X41122.
[22] S. M. Wulfsberg, B. E. Koel, S. L. Bernasek, *Surf. Sci.* **2016**, *651*, 120–127. https://doi.org/10.1016/j.susc.2016.04.003.
[23] T. Liu, J. P. Vivek, E. W. Zhao, J. Lei, N. Garcia-Araez, C. P. Grey, *Chem. Rev.* **2020**, *120*(14), 6558–6625. https://doi.org/10.1021/acs.chemrev.9b00545.
[24] I. Ruiz de Larramendi, N. Ortiz-Vitoriano, *Front. Chem.* **2020**, *8*, 605. https://doi.org/10.3389/fchem.2020.00605.
[25] E. L. Clennan, A. Pace, *Tetrahedron* **2005**, *61* (28), 6665–6691. https://doi.org/10.1016/j.tet.2005.04.017.
[26] P. R. Ogilby, *Chem. Soc. Rev.* **2010**, *39* (8), 3181. https://doi.org/10.1039/b926014p.
[27] A. A. Krasnovsky, *J. Photochem. Photobiol. Chem.* **2008**, *196* (2–3), 210–218. https://doi.org/10.1016/j.jphotochem.2007.12.015.
[28] A. A. Gorman, M. A. J. Rodgers, *Chem. Soc. Rev.* **1981**, *10*(2), 205. https://doi.org/10.1039/cs9811000205.
[29] R. Schmidt, *Photochem. Photobiol.* **2007**, *82* (5), 1161–1177. https://doi.org/10.1562/2006-03-03-IR-833.
[30] C. Schweitzer, R. Schmidt, *Chem. Rev.* **2003**, *103* (5), 1685–1758. https://doi.org/10.1021/cr010371d.
[31] R. Schmidt, E. Afshari, *Berichte Bunsenges. Für Phys. Chem.* **1992**, *96* (6), 788–794. https://doi.org/10.1002/bbpc.19920960610.
[32] P. B. Merkel, D. R. Kearns, *J. Am. Chem. Soc.* **1972**, *94* (3), 1029–1030. https://doi.org/10.1021/ja00758a071.
[33] J. Wandt, P. Jakes, J. Granwehr, H. A. Gasteiger, R.-A. Eichel, *Angew. Chem.* **2016**, *128* (24), 7006–7009. https://doi.org/10.1002/ange.201602142.
[34] A. Schürmann, B. Luerßen, D. Mollenhauer, J. Janek, D. Schröder, *Chem. Rev.* **2021**, *121* (20), 12445–12464. https://doi.org/10.1021/acs.chemrev.1c00139.
[35] M. Hong, H. R. Byon, *Batteries & Supercaps* **2021**, *4* (2), 286–293. https://doi.org/10.1002/batt.202000210.
[36] V. S. Bryantsev, M. Blanco, F. Faglioni, *J. Phys. Chem. A* **2010**, *114* (31), 8165–8169. https://doi.org/10.1021/jp1047584.
[37] V. S. Bryantsev, *Theor. Chem. Acc.* **2012**, *131* (7), 1250. https://doi.org/10.1007/s00214-012-1250-7.
[38] S. Mondal, R. B. Jethwa, B. Pant, R. Hauschild, S. A. Freunberger, *Faraday Discuss.* **2024**, *248*, 175–189.10.1039/D3FD00088E .
[39] A. Zaichenko, D. Schröder, J. Janek, D. Mollenhauer, *Chem. Eur. J.* **2020**, *26* (11), 2395–2404. https://doi.org/10.1002/chem.201904110.
[40] S. Mai, P. Marquetand, L. González, *WIREs Comput. Mol. Sci.* **2018**, *8*(6). https://doi.org/10.1002/wcms.1370.
[41] S. Mai, M. Richter, "SHARC2.1: surface Hopping Including Arbitrary Couplings - Program Package for Non-Adiabatic Dynamics". Sharc-Md.Org **2019**.
[42] M. Richter, P. Marquetand, J. González-Vázquez, I. Sola, L. González, *J. Chem. Theory Comput.* **2011**, *7* (5), 1253–1258. https://doi.org/10.1021/ct1007394.
[43] M. Richter, P. Marquetand, J. González-Vázquez, I. Sola, L. González, [*J. Chem. Theory Comput.* **2011**, *7*, 1253–1258]. *J. Chem. Theory Comput.* **2012**, *8* (1), 374–374. https://doi.org/10.1021/ct2005819.
[44] J. C. Tully, *J. Chem. Phys.* **1990**, *93*(2), 1061–1071. https://doi.org/10.1063/1.459170.
[45] J. C. Tully, R. K. Preston, *J. Chem. Phys.* **1971**, *55*(2), 562–572. https://doi.org/10.1063/1.1675788.
[46] M. Richter, P. Marquetand, J. González-Vázquez, I. Sola, L. González, *J. Phys. Chem. Lett.* **2012**, *3* (21), 3090–3095. https://doi.org/10.1021/jz301312 h.
[47] L. Martínez-Fernández, J. González-Vázquez, L. González, I. Corral, *J. Chem. Theory Comput.* **2015**, *11* (2), 406–414. https://doi.org/10.1021/ct500909a.
[48] S. Gómez, M. Heindl, A. Szabadi, L. González, *J. Phys. Chem. A* **2019**, *123* (38), 8321–8332. https://doi.org/10.1021/acs.jpca.9b06103.
[49] B. R. Henry, M. Kasha, *Annu. Rev. Phys. Chem.* **1968**, *19* (1), 161–192. https://doi.org/10.1146/annurev.pc.19.100168.001113.
[50] W. D. Allen, D. A. Horner, R. L. Dekock, R. B. Remington, H. F. Schaefer, *Chem. Phys.* **1989**, *133* (1), 11–45. https://doi.org/10.1016/0301-0104(89)80097-7.
[51] A. Pierini, S. Brutti, E. Bodo, *J. Phys. Chem. A* **2021**, *125* (42), 9368–9376. https://doi.org/10.1021/acs.jpca.1c07255.
[52] I. Fdez, Galván, M. Vacher, A. Alavi, C. Angeli, F. Aquilante, J. Autschbach, J. J. Bao, S. I. Bokarev, N. A. Bogdanov, R. K. Carlson, L. F. Chibotaru, J. Creutzberg, N. Dattani, M. G. Delcey, S. S. Dong, A. Dreuw, L. Freitag, L. M. Frutos, L. Gagliardi, F. Gendron, A. Giussani, L. González, G. Grell, M. Guo, C. E. Hoyer, M. Johansson, S. Keller, S. Knecht, G. Kovačević, E. Källman, G. Li Manni, M. Lundberg, Y. Ma, S. Mai, J. P. Malhado, P. Å. Malmqvist, P. Marquetand, S. A. Mewes, J. Norell, M. Olivucci, M. Oppel, Q. M. Phung, K. Pierloot, F. Plasser, M. Reiher, A. M. Sand, I. Schapiro, P. Sharma, C. J. Stein, L. K. Sørensen, D. G. Truhlar, M. Ugandi, L. Ungur, A. Valentini, S. Vancoillie, V. Veryazov, O. Weser, T. A. Wesołowski, P.-O. Widmark, S. Wouters, A. Zech, J. P. Zobel, R. Lindh, *J. Chem. Theory Comput.* **2019**, *15* (11), 5925–5964. https://doi.org/10.1021/acs.jctc.9b00532.
[53] F. Aquilante, J. Autschbach, A. Baiardi, S. Battaglia, V. A. Borin, L. F. Chibotaru, I. Conti, L. De Vico, M. Delcey, I. Fdez, Galván, N. Ferré, L. Freitag, M. Garavelli, X. Gong, S. Knecht, E. D. Larsson, R. Lindh, M. Lundberg, P. Å. Malmqvist, A. Nenov, J. Norell, M. Odelius, M. Olivucci, T. B. Pedersen, L. Pedraza-González, Q. M. Phung, K. Pierloot, M. Reiher, I. Schapiro, J. Segarra-Martí, F. Segatta, L. Seijo, S. Sen, D.-C. Sergentu, C. J. Stein, L. Ungur, M. Vacher, A. Valentini, V. Veryazov, *J. Chem. Phys.* **2020**, *152*(21), 214117. https://doi.org/10.1063/5.0004835.
[54] B. O. Roos, R. Lindh, P.-Å. Malmqvist, V. Veryazov, P.-O. Widmark, *J. Phys. Chem. A* **2004**, *108* (15), 2851–2858. https://doi.org/10.1021/jp031064+.
[55] B. O. Roos, V. Veryazov, P.-O. Widmark, *Theor. Chem. Acc.* **2004**, *111* (2–6), 345–351. https://doi.org/10.1007/s00214-003-0537-0.
[56] A. Pierini, S. Brutti, E. Bodo, *ChemPhysChem* **2020**, *21* (18), 2060–2067. https://doi.org/10.1002/cphc.202000318.
[57] T. Dunning, *J. Chem. Phys.* **1971**, *55* (2), 716–723. https://doi.org/10.1063/1.1676139.

[58] J. P. Dahl, M. Springborg, *J. Chem. Phys.* **1988**, *88* (7), 4535–4547. https://doi.org/10.1063/1.453761.
[59] M. Barbatti, K. Sen, *Int. J. Quantum Chem.* **2016**, *116*(10), 762–771. https://doi.org/10.1002/qua.25049.
[60] G. Granucci, M. Persico, A. Zoccante, *J. Chem. Phys.* **2010**, *133*(13), 134111. https://doi.org/10.1063/1.3489004.
[61] T. Kato, *J. Phys. Soc. Jpn.* **1950**, *5* (6), 435–439. https://doi.org/10.1143/JPSJ.5.435.
[62] E. Mourad, Y. K. Petit, R. Spezia, A. Samojlov, F. F. Summa, C. Prehal, C. Leypold, N. Mahne, C. Slugovc, O. Fontaine, S. Brutti, S. A. Freunberger, *Energy Environ. Sci.* **2019**, *12* (8), 2559–2568. https://doi.org/10.1039/C9EE01453E.
[63] S. Dong, S. Yang, Y. Chen, C. Kuss, G. Cui, L. R. Johnson, X. Gao, P. G. Bruce, *Joule* **2022**, *6* (1), 185–192. https://doi.org/10.1016/j.joule.2021.12.012.
[64] J. K. Nørskov, J. Rossmeisl, A. Logadottir, L. Lindqvist, J. R. Kitchin, T. Bligaard, H. Jónsson, *J. Phys. Chem. B* **2004**, *108*(46), 17886–17892. https://doi.org/10.1021/jp047349j.

Manuscript received: February 28, 2024
Revised manuscript received: June 11, 2024
Accepted manuscript online: July 29, 2024
Version of record online: November 20, 2024